Climate Data Record (CDR) Program

Climate Algorithm Theoretical Basis Document (C-ATBD)

Mean Layer Temperature - UAH

CDR Program Document Number: CDRP-ATBD-0108
Configuration Item Number: 01B-10
Revision 3 / April 13, 2017

REVISION HISTORY

Rev.	Author	DSR No.	Description	Date
1	John Christy, UAH	DSR-114	Initial Submission to CDR Program	09/22/2011
2	John Christy, UAH	DSR-724	Updated for CR-0050	02/28/2017

TABLE of CONTENTS

LIST of FIGURES

1. Introduction

1.1 Purpose

The purpose of this document is to describe the algorithms and procedures submitted to the National Centers for Environmental Information (NCEI) by Roy W. Spencer and John R. Christy that are currently used as processing steps leading to creating the Mean Layer Temperature - UAH Climate Data Record (CDR) that consists of Mean Layer Temperatures (MLTs) for the lower troposphere (TLT), middle troposphere (TMT), the tropopause layer (TTP new in version 6.0) and lower stratosphere (TLS), using the Microwave Sounding Units (MSU) and the Advanced Microwave Sounding Units (AMSU).

The actual algorithm is defined by the computer program (code) that accompanies this document, and thus the intent here is to provide a guide to understanding that algorithm, from both a scientific perspective and in order to assist a software engineer performing an evaluation of the code.

1.2 Definitions

Following is a summary of the symbols used to define the algorithm.

The satellite-observed quantity which is interpreted as a measure of deep-layer average atmospheric temperature is the microwave brightness temperature (Tb) measured within the 50-60 GHz oxygen absorption complex. For specific frequencies in this band where the atmospheric absorption is so strong that the Earth's surface is essentially obscured, the rate of thermal emission by the atmosphere is very nearly proportional to the temperature of the air. For example, the lower stratospheric temperature product (TLS) is almost 100% composed of thermal emission from atmospheric molecular oxygen.

In the more general case, the brightness temperature also depends upon the emissivity of the object being measured, as well as its temperature,

$$T_b = \varepsilon\, T \qquad (1)$$

As a result, the middle tropospheric temperature (TMT) and lower tropospheric temperature (TLT) and to a small extent the tropopause layer (TTP) products have a component of surface emission "shining through" the atmospheric layer being sensed which, depending upon the surface, may or may not be directly proportional to temperature of that surface.

These sources of contamination have been found to be relatively small (but not totally negligible) in the *time-variations* of the TLT, TMT and TTP products, so throughout this document Tb variations will be assumed to be loosely proportional to temperature variations.

(Note: While some call the calibrated satellite-based measurement an "antenna temperature" [Ta] unless antenna pattern corrections are made, such corrections have

little impact on climate data records, and so we will not make a distinction between Ta and Tb.)

1.3 Referencing this Document

This document should be referenced as follows:

Mean Layer Temperature - UAH - Climate Algorithm Theoretical Basis Document, NOAA Climate Data Record Program CDRP-ATBD-0108 Rev. 3 (2017). Available at https://www.ncdc.noaa.gov/cdr/fundamental/mean-layer-temperature-uah

1.4 Document Maintenance

When requested by NOAA, if there have been any changes in procedures required for the production of the products or if the description of procedures has inadvertent omissions or errors, we will update this C-ATBD.

2. Observing Systems Overview

2.1 Products Generated

There are four atmospheric layers for which intermediate products are processed:

(1) **TLT** (lower-tropospheric deep-layer average temperature, computed as a linear combination of the values of **TMT**, **TTP** and **TLS: TLT** = 1.538x**TMT** – 0.548x**TTP +** 0.010x**TLS**). The coefficient values were determined to maximize the weighting function below the tropopause, with virtually no contribution from the stratosphere, and

(2) **TMT** (mid-tropospheric deep-layer temperature, computed as the value of the T_b which intersects the polynomial fit through the observed monthly average gridpoint T_b along all 6 view angles of MSU2 at 21.59° and the T_b which intersects the polynomial fit of the observed T_b along all 15 view angles of AMSU5 at 38.31°), and

(3) **TTP** (deep-layer centered on tropopause computed as the value of the T_b which intersects the polynomial fit through the observed monthly average gridpoint T_b along all 6 view angles of MSU3 at 21.59° and the T_b which intersects the polynomial fit of the observed T_b along all 15 view angles of AMSU7 at 13.18°), and

(4) **TLS** (lower-stratospheric deep layer temperatures, computed as the value of the T_b which intersects the polynomial fit through the observed monthly average gridpoint T_b along all 6 view angles of MSU4 at 21.59° and the T_b which intersects the polynomial fit of the observed T_b along all 15 view angles of AMSU9 at 36.31°).

For each of these four atmospheric layers, there are monthly 2.5 deg. latitude and longitude absolute and anomaly T_bs produced. Global and regional averages are subsequently calculated and provided within the netCDF data file.

2.2 Instrument Characteristics

The deep layer temperature products described here come from measurements produced by Advanced Microwave Sounding Units (AMSU-As, hereafter "AMSU") flying on NOAA polar orbiting satellites (operating since mid-1998), on NASA's Aqua satellite (operating since mid-2002) and on the European MetOp-B satellite (operating since 2013). Before AMSU, the Microwave Sounding Units (MSUs) flew on the NOAA polar orbiters since late 1978.

These instruments are cross-track through-nadir scanning externally-calibrated passive microwave radiometers. They make brightness temperature measurements at microwave frequencies within the 50-60 GHz oxygen absorption complex, and (in the case of AMSU) at a few microwave frequencies above and below that absorption complex.

The radiometers are designed to measure the weak thermal emission by molecular oxygen (O_2) in the atmosphere. The atmospheric concentration of O_2 is spatially

uniform and very stable over time at approximately 20.95%, and so it is a good "tracer" for remotely monitoring of atmospheric temperature variations from space.

From a practical perspective, however, the atmospheric temperature measurement (at least in the troposphere, where weather and climate variations are concentrated) cannot be made without also measuring at least some amount of thermal emission from the Earth's surface shining up through the atmosphere for layers below TLS. Therefore, more surface-sensitive channels were included in the AMSU sensor design in order to better correct for this contaminating influence on the atmospheric measurements.

This is important for the wide range of surface backgrounds in different regions, since the intended use of AMSU for monitoring regional temperature variations for input into numerical weather prediction models. We do not, however, perform any such corrections to our products.

The MSU (AMSU) makes measurements for 4 (15) different channels at 11 (30) footprints within each scan, with a nominal footprint spatial resolution of about 110 (50) km at nadir. Scans are made approximately every 150 (50) km along the satellite track.

The measurements are calibrated as "brightness temperatures" (T_b) on each scan of the instrument using a 2-point calibration method. Deep-space views made during every scan of the instrument provide the cold reference point (assumed to be near 3 K), and the hot calibration point is provided by a high-emissivity unheated calibration target internal to the instrument whose temperature is monitored with redundant platinum resistance thermometers (PRTs).

The Earth-viewing measurements are calibrated by interpolating between the cold space view and the warm target view measurements. The AMSU instruments had detailed pre-launch characterization of the instruments, and we use the calibration equation coefficients in the Level 1b orbit files provided by NESDIS, using the calibration equation provided in the document listed below. In the case of the older MSU instruments, we ignored the NOAA-provided calibration equations, and perform our own linear interpolation with an adjustment to account for variations in the instrument temperature, since nonlinearities in the sensor response were not well documented pre-launch.

Much more information on the characteristics of the AMSUs, their calibration, and Level 1b data format can be found at http://www.ncdc.noaa.gov/oa/pod-guide/ncdc/docs/klm/index.htm. Similar details for the MSUs can be found at http://www.ncdc.noaa.gov/oa/pod-guide/ncdc/docs/podug/index.htm.

3. Algorithm Description

3.1 Algorithm Overview

The goal is to provide a long-term record of space- and time-averaged deep-layer average temperatures for four atmospheric layers, while minimizing errors due to incomplete spatial sampling, calibration, the varying time-of-day of the measurements, contamination by surface effects on the measurements, and decay of the satellites' orbits over time. The easiest part of this process is the actual calibration of the instrument measurements, which in the absence of contaminating influences from the Earth's surface or hydrometeors in the atmosphere, provides T_b's which are directly proportional to air temperature, which is what we desire to measure.

3.2 Processing Outline

Most of the procedures used in processing of UAH MLT v6.0 products are described in general terms in Spencer et al. 2017, which is listed in the References section at the end.

The following flow diagrams show the components of the data processing. Boxes with dotted outlines represent data files, while those with solid outlines represent either Perl or FORTRAN codes. Example data file names are in parentheses. All channels are generated from the same code, thus we show here only one flow diagram for TLT, TMT, TTP and TLS.

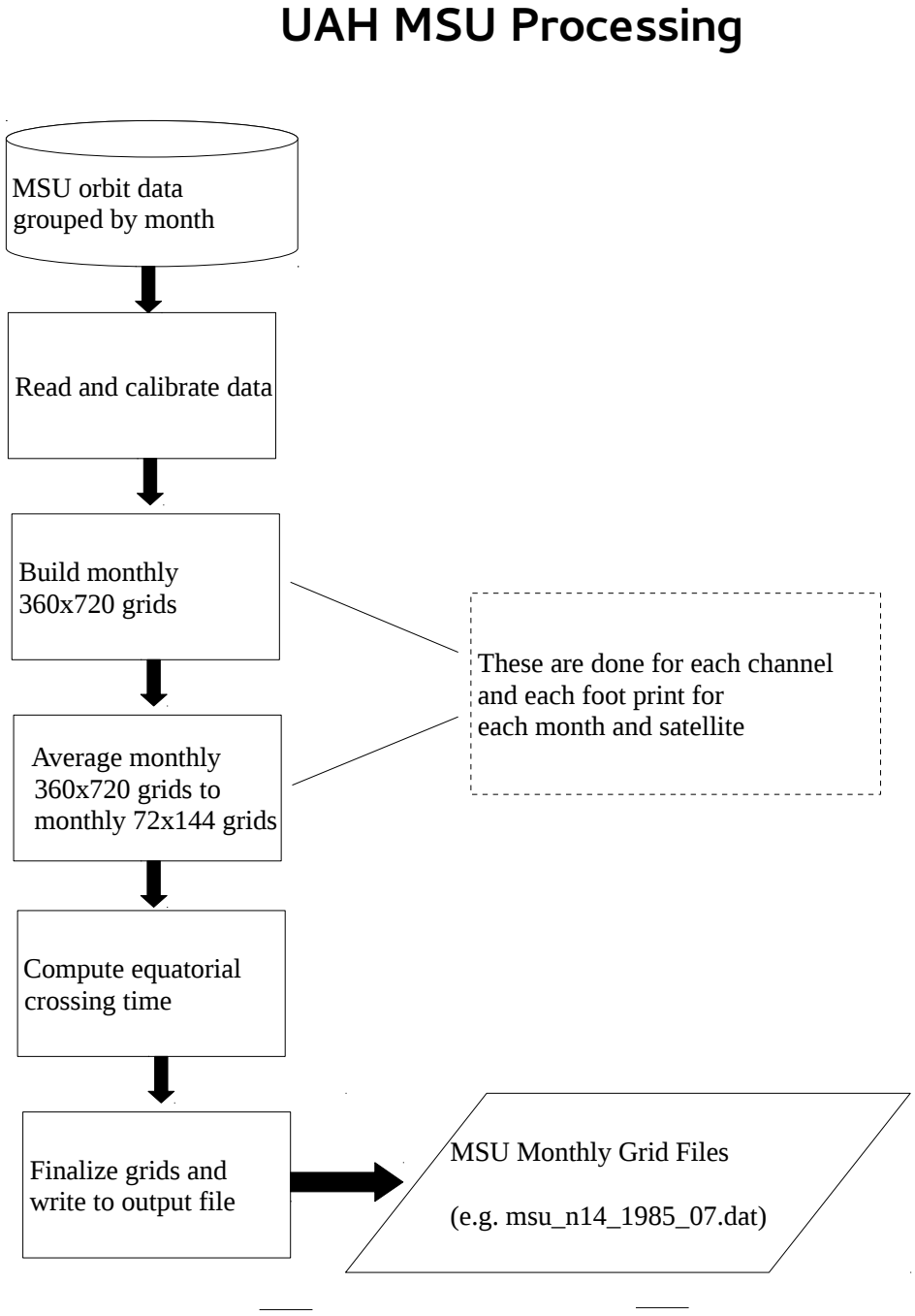

Figure 1: Processing flow for the MSU data processing.

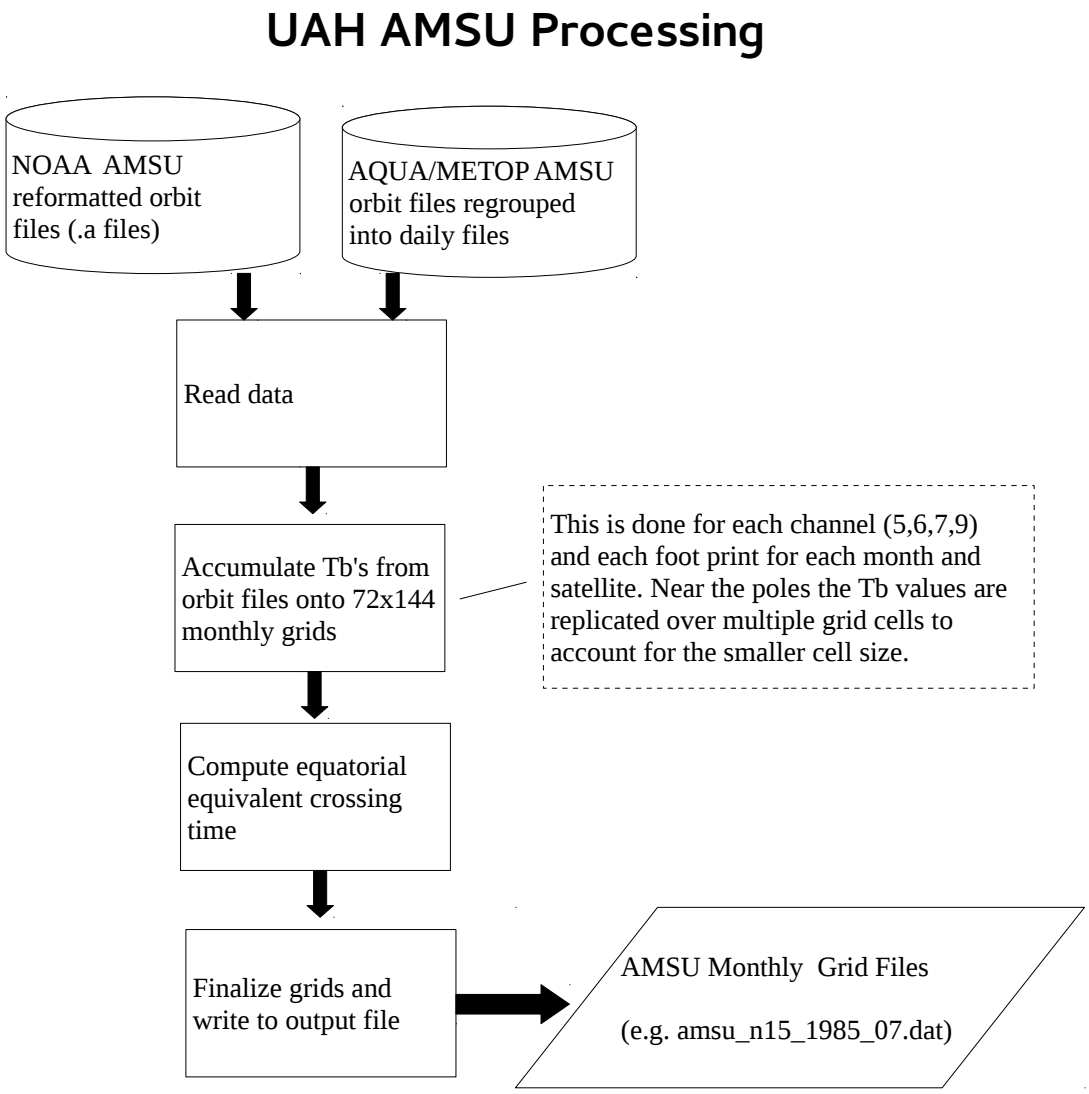

Figure 2: Processing flow for the AMSU data processing.

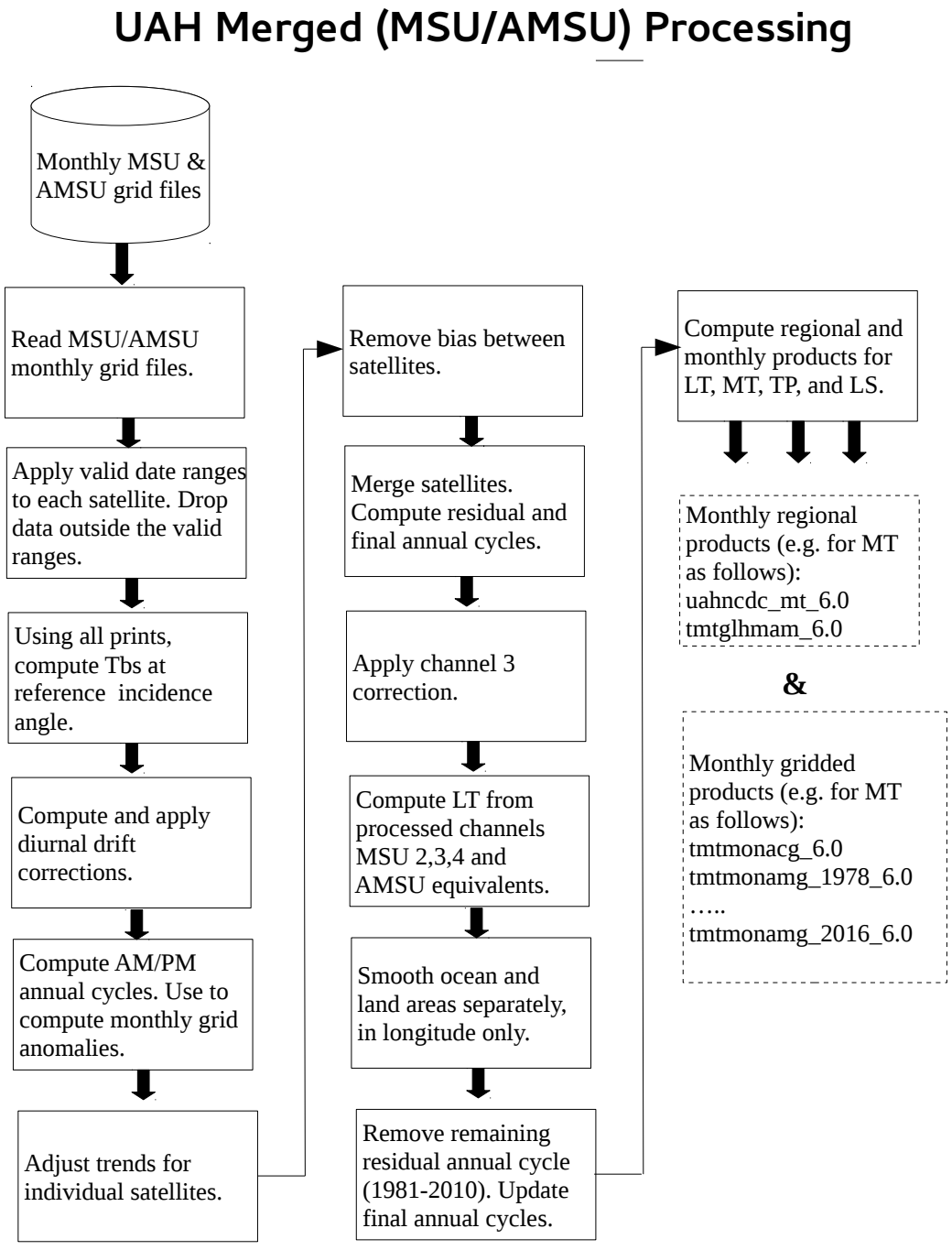

Figure 3: Processing flow for the merging of MSU and AMSU data into the final products.

3.2.1 Gathering of the Latest Month's Worth of Data

The UAH processing procedures are implemented usually the first week of each new month after we have determined that all of the AMSU data files have been obtained for the previous month so that a monthly update of the UAH products can be performed. [MSU files ceased to be produced after NOAA-14.]

3.2.2 Creating Files of Filenames

For the AMSU orbit files from the NOAA satellites, we run a Perl program "mk_files2.perl" which creates a single file of one month of 28 to 31 daily filenames, while each daily file contains a list of approximately 14 AMSU Level 1b orbit file names. These filenames are generated by reading a specified subdirectory and finding orbit files that fall within the user specified month, for a single user specified satellite.

For the Aqua AMSU data, which have a different format and come from a different data provider, there is only one file of global AMSU data per day, so a file of 28 to 31 daily filenames is generated manually.

3.2.3 Computing Monthly Gridded Values

In the case of the MSU instruments, the T_bs are calculated by the linear relationship between sensor counts at the cold-space view and the hot-target view. The counts of the Earth-view are simply linearly interpolated to the T_b from this relationship. A further adjustment to MSU readings is made to account for the linear relationship between the instrument's temperature and the Earth-view temperature (so-called "hot-target" adjustment.) In the case of the AMSU instruments, the T_bs are calculated from the NESDIS-supplied calibration equation and no hot-target adjustment is required.

The calibrated T_bs are binned into monthly grid boxes for each view angle (6 view angles for MSU and 15 for AMSU), as many T_bs per view angle as are available for that month. A second order polynomial is fitted to the view-angle vs. T_b array and then the T_b for the required view angle is determined from the polynomial (see Section 2.1 above for view angle values). This eliminates the need for limb corrections and orbit decay adjustments.

Special consideration was given for MSU3 (used in TTP) for NOAA-6. For unknown reasons, this channel developed calibration drift so that its values were not credible. To adjust the data, Version 6.0 monthly anomalies for MSU channels 2, 3, and 4 were analyzed post-NOAA-6 to determine the average relationship expected between channel 3 as a linear combination of channels 2 and 4. This regression relationship was the applied to the NOAA-6 channel 2 and 4 data to obtain an estimate of the channel 3 time series of anomalies. This regression estimate was then differenced with the NOAA-6 measured channel 3 anomalies to arrive at a drift estimate for NOAA-6 channel 3, which was then subtracted from the original calibrated data before further processing.

3.2.4 Diurnal Drift Correction

As the orbit decays due to friction in the thin atmosphere for spacecraft which do not have propulsion capability to be kept in a consistent crossing-time orbit, the sensor will measure temperature at new (later or earlier) local times on the Earth. This introduces spurious temperature drifts that must be accounted for, especially over land. The effect is calculated directly by comparing the T_bs of a drifting spacecraft vs. a non-drifting spacecraft. The result of such comparison is a relationship of temperature change vs. time drift from the initial crossing time. For the "a.m." ("p.m.") orbiters the drifting spacecraft was NOAA-15 (NOAA-18) and the non-drifting was AQUA (NOAA-19 during first four years of overlap). Not utilized were NOAA-16 (badly drifting channel 5 sensor) and NOAA-17 (power surge that disabled scan motors). In order to reduce spatial noise in the resulting gridpoint diurnal drift coefficients, these diurnal calculations for land grids were subsequently also made dependent on altitude and average annual rainfall as these two characteristics tended to modify the relationship (greater diurnal change for high altitude or dry regions). This correction is applied to each of the three primary products (TMT, TTP and TLS) of both MSU and AMSU sensors recognizing that TLT, as a derived product, will be diurnally corrected as a result. Example of global images of the resulting diurnal drift coefficients are shown in Spencer et al., 2017.

For the MSU time series, there remained small trend differences between the overlapping periods for NOAA-11 and NOAA-14 relative to the other co-orbiting satellites. These were minimized by an objective algorithm that calculated a trend adjustment that would minimize the trend-difference between these two "p.m." sensors and the two "a.m." satellites with which they overlapped (NOAA-10 and -12 for NOAA-11, and NOAA-12 and -15 for NOAA-14). The trend adjustment was applied to all grids.

3.2.5 Merging The Individual Satellite Gridded Data

The data at this point are sets of 144x72 (2.5 degree grid) arrays of monthly temperatures for each satellite for three primary channels (TMT, TTP and TLS). The data are merged by eliminating intersatellite biases calculated during the overlapping periods of operation. Because there were always at least two satellites operating, there is a pathway for bias removal from the first satellite to the last. Once the biases are removed, a mean annual cycle for 1981-2010 is calculated. From the arrays of the three channels is calculated the derived product TLT (see Section 2.1 above) at each grid with its mean annual cycle. Gridded anomalies are then calculated from the original arrays of absolute temperatures relative to the 1981-2010 period.

3.3 Algorithm Input

3.3.1 Primary Sensor Data

The primary sensor data are the MSU and AMSU-A Level 1b data files as provided by NOAA/NESDIS, and the AMSU-A data provided by NASA as part of the Aqua AIRS dataset. The NOAA AMSU data input into these programs are already calibrated as

Tb's and are contained in "dot-a" (.a) files generated by Danny Braswell, who has also separately provided code to NCDC which generates the dot-a files from the original NOAA/NESDIS Level 1b orbit files.

The Aqua AMSU data files used as input to these programs are reformatted versions of the HDF data files obtained from NASA, the code for which has also been provided separately by Danny Braswell.

3.3.2 Ancillary Data

1) A static ASCII file ("ih2o50.txt") of global gridpoint percent water coverage values, which is used for the limb-correction procedures. This file has values of percent water coverage from 0 to 100, averaged on a ~50 km spatial scale, and stored on a 1/6 deg. latitude/longitude grid. We computed these values from an old original Fleet Numerical Oceanographic Center (FNOC) 1/6 deg. percent water coverage dataset which we believe is no longer in existence.

2) Satellite-specific orbital altitude files are used as input to. These files have altitudes computed at 1-minute time resolution from 2-line-element sets during the satellite mission to date, with future altitudes estimated up to one year in advance. The code to create these orbit altitude files has been provided separately by Danny Braswell.

3.3.3 Derived Data

Not Applicable

3.3.4 Forward Models

Not Applicable

3.4 Theoretical Description

Most of the physics and radiative transfer concepts have already been described in previous sections. A few additional details and clarifications follow.

3.4.1 Physical and Mathematical Description

The algorithm is based upon the fact that passive microwave brightness temperatures measured in the 50-60 GHz oxygen absorption band are directly proportional to air temperature, with almost a 1:1 proportionality. This means that the Tb anomalies computed as the final products are approximately equal to air temperature anomalies, for deep layers of the atmosphere as defined by the weighting function for each channel. There is some non-negligible influence of surface temperature and emissivity, although this is small and difficult to adjust for.

The radiometer calibration is linear for the MSU instruments and only slightly non-linear for the AMSU instruments; the calibrated brightness temperature is simply an interpolation between the cold space view radiometer digital counts (assumed near 2.7

Kelvin) and on-board warm target temperature digital counts (temperature measured by redundant platinum resistance thermometers) to the brightness temperature corresponding to the Earth view radiometer digital counts.

Because each of the scan angles of the thru-nadir scanning instruments provide atmospheric weighting functions which are at somewhat different altitudes, we use a novel method of measuring monthly average Tb at each scan angle separately for any given gridpoint location, and then use polynomial regression to interpolate to a desired "reference" Earth incidence angle. This provides our best estimate of the average Tb at that gridpoint for the atmospheric layer represented by that view angle.

3.4.2 Data Merging Strategy

The general idea is that the individual instruments need time-dependent adjustments for diurnal drift and the impact of solar heating of the sensor as it drifts to different crossing times where components of the instrument receive time-varying solar radiation. With these adjustments applied, the last step is to de-bias all satellite time series relative to each other, then the anomalies are merged.

3.4.3 Numerical Strategy

Due to the simplicity of the problem described above, there are no complicated numerical methods or iterative procedures necessary in the algorithm. All computations are based upon simple arithmetic averaging or statistical linear regression.

3.4.4 Calculations

The processing flow of the code is already summarized in the previous flowcharts, and so the following descriptions are largely redundant with that. To add more detail than the plain-language flowcharts would verge on repeating the actual code. Nevertheless, the following discussion might help understand some of the more important sequential steps in the processing.

The raw measurements made by the MSU and AMSU instruments are radiometer output voltages digitized into digital counts. These digital count measurements are for the Earth-viewing measurements, a cold calibration view of deep space, and a warm calibration view of an on-board calibration target. For each scan line of data the instrument makes as it scans across the orbital sub-track, the calibration information for that scan is used to calibrate the Earth-viewing data into brightness temperatures.

For the older (MSU) instruments, a warm target correction is necessary to adjust for the observed dependence of the calibrated Tb on the warm calibration target temperature. This is estimated by regression of Tb differences between simultaneously

operating satellites against their target temperature differences. The resulting regression coefficients minimize the monthly Tb differences over the tropical oceans on a monthly basis, and those coefficients are used as an additional step in the calibration procedure for the MSU Tb.

For each month and 2.5 deg. gridpoint, average Tb are computed for each instrument view angle separately, for each satellite instrument separately. Then for each gridpoint, polynomial regression is used to estimate the month-average Tb at a desired, nominal Earth incidence angle. This requires each of the view angles for that satellite and month to have an Earth incidence angle computed from satellite orbit ephemeris data. The nominal Earth incidence angles were chosen to be intermediate between nadir and limb, while taking into account slight difference in the MSU and AMSU channel frequencies (and thus weighting function altitudes).

This results in monthly average grids of Tb for the nominal layers we monitor: mid-troposphere (TMT), tropopause (TTP), and lower stratosphere (TLS). A linear combination of these layers produces the lower troposphere (TLT) product. These monthly grids are archived during each monthly update of the dataset, and need not be recomputed each time.

Diurnal drift adjustments are then applied to all grids based upon statistical analysis of the aforementioned grids by regressing Tb differences against local ascending node time differences at each gridpoint between NOAA-15 (drifting “7:30” satellite) and Aqua (non-drifting) to get drift coefficients (deg. C/hr) for the 7:30 satellites as a function of nominal local observation time. Similarly, regressions of NOAA-18 (drifting “1:30” satellite) against NOAA-19 (non-drifting “1:30” satellite) provide diurnal drift coefficients for all of the 1:30 satellites as a function of nominal local observation time. Since these diurnal drift coefficients were found to be somewhat noisy when displayed as maps, an additional diurnal drift step was added involving regression inter-satellite Tb differences against terrain altitude and climatological precipitation amounts, resulting in an ancillary lookup file of drift coefficients (see Section 3.4.6 for more detail).

Next, “7:30” (also termed “am”) and “1:30” (also termed “pm”) gridpoint annual cycles are computed for specific satellites and date ranges, and then anomalies about those annual cycles are computed (anomaly = raw minus cycle). Trend and bias adjustments are then performed for the satellites separately. Then simultaneously operating satellites are merged (averaged together), and a residual annual cycle is computed. Modest smoothing of the resulting anomalies is performed in the longitudinal direction only, keeping land and ocean separate. Compute the remaining average annual cycle (1981-2010) at each

gridpoint and remove it from the entire time series to arrive at monthly anomalies. Finally, we produce gridpoint and regional output file products for all four layers (TLT, TMT, TTP, and TLS).

3.4.5 Look-Up Table Description

The necessary static ancillary input datasets have already been described.

3.4.6 Parameterization

The only portion of our algorithm that could be considered as "parameterization" is the use of climatological precipitation data and a terrain altitude database as inputs to our diurnal drift adjustment procedure. As the satellites drift through the diurnal cycle, the observed temperature changes, since it is warmer during the day than at night (at least in the troposphere). This diurnal drift effect is magnified for dry regions (deserts) and at high elevations, where the solar-heated land extends unusually far up into the atmospheric weighting function. Our estimation of diurnal drift (change in Tb per hour of observation time drift) by simply comparing a drifting satellite with a non-drifting satellite is noisy at the gridpoint and calendar month level. To reduce the noise, we parameterize a portion of the diurnal drift by adding terrain altitude and climatological gridpoint precipitation information (Global Precipitation Climatology Project calendar monthly precipitation averages for 1981-2010) to the regression estimation of diurnal drift.

3.4.7 Algorithm Output

The various output files have been described above and can be seen in Figs. 1-3.

4. Test Datasets and Outputs

4.1 Test Input Datasets

Not Applicable – all input datasets are operational datasets

4.2 Test Output Analysis

4.2.1 Reproducibility

As the code was developed and executed, output and code for each version were saved. Then, with each iteration, the new output was directly compared with the output from previous runs to assure reproducibility and stability of processing of input files and production of output files.

4.2.2 Precision and Accuracy

The precision and accuracy have been discussed in previous publications. The key quantity for our research is not the absolute accuracy of the measurement, but the precision over time, i.e. the error in trends. There are up to 1 K differences in the different instruments that have been launched, but once these intersatellite biases are removed, the measurements show a high level of agreement on departures from their respective mean values over time. From research publications previously we anticipate a precision value for annual global anomalies of ±0.1 K and of the global trend at ±0.04 K decade^{-1}.

4.2.3 Error Budget

Intersatellite bias	±0.01 K (globe)	Several hundred to several thousand simultaneous daily-mean observations are made for co-orbiting satellites, so that the mean bias is known to high precision
Diurnal Correction	±0.02 K/yr/sat (globe)	The diurnal correction is empirically determined per latitude band and land/ocean surface type. This reduces the number of empirical observations available for the calculation of the diurnal drift per gridpoint and thus reduces the level of precision. Globally however, these random errors tend to average out. The value here is conservative and would apply only to short periods of the time series, not to the entire time series. Testing the UAH global trends over 38 years against balloon and Reanalyses indicates the overall error is likely on the order of ±0.02 K decade^{-1}.
Hot target temperature correction (MSU only)	±0.02 K/decade (globe)	Shorter overlap periods will lead to greater error in calculating the necessary correction for the hot target variations on the calibration equation. Each overlap produces its unique correction factor so that random error will work to limit the overall error in the time series.
Unknown Calibration drifts	±0.02 K/decade (global)	We have published evidence that at least one satellite (NOAA-12) may have a slight drift in the sensor for reasons unrelated to the corrections described above. This drift introduces a spurious warming to the time series. It is possible other instruments (though we have no strong information as of yet) may also have uncorrected drifts.

4.2.4 Output Dataset Quality Evaluation

The quality of the intermediate data products described here was optimized over a period of many years, mostly between 1990 and 2000. The Version 6 procedures represent the accumulated knowledge gained by ourselves, and relayed to us by users, which then result in our best attempts at correcting known problems in the satellite data, and most efficiently estimates monthly gridpoint temperature anomalies for the relevant atmospheric layers with the greatest signal-to-noise.

Qualitative evaluation of the improvements achieved in Version 6 was done by examining imagery of monthly gridpoint anomalies as we were testing alternative procedures, to identify unacceptable levels of geographic noise in those fields. This was an iterative process and helped us optimize the final procedures, such as our new polynomial fitting of all of the different view angles of data to estimate the Tb at a desired nominal view

angle. Spatial continuity of monthly anomaly fields across land-ocean boundaries was a particularly stringent test during our optimization process.

Quantitative evaluation of the Version 6 products continues with comparisons to radiosonde data, initial results of which are contained in Spencer et al., 2017, and intersatellite signal/noise calculations.

5. Practical Considerations

5.1 Numerical Computation Considerations

This section outlines the procedure we follow monthly to create version 6 updates for the previous month. It is a more verbose version of the primary README file included with the software. We use this README file as a checklist each month when updating the data products.

This section is divided into 3 parts: 1) updating the monthly grid files, 2) updating the two-line-element (TLE) database and computing satellite incidence angles, and 3) merging the satellites and creating the final output products. The directory paths used in what follows are for our processing computer. They will need to be modified to match the installation of the software on your computer. Our host computer is Linux based and runs the latest version of Centos. Compilation is done with the Portland Group Fortran 95 compiler.

5.2 Programming and Procedural Considerations

5.2.1 Updating the Monthly Grid Files

Our version 6 processing currently makes monthly updates using only AMSU-A's on NOAA 18 and 19. The satellite orbit files are downloaded automatically by our data center as soon as available. We have a script that reformats them into a simpler format and renames them by appending ".a" to the end of each file name. These are placed in the directory /rgroup/ams/dot_a_files/.

The next step is to use the program "count_orbit_files.perl" to determine if the orbit file and dot-a-file inventory is complete. An example of running this program for N18 and N19 is:

* count_orbit_files.perl n18 2016 214 244

* count_orbit_files.perl n19 2016 214 244

where the arguments are satellite, year, month, beginning julian day and ending julian day.

If orbit files are missing, they must be downloaded from www.class.ngdc.noaa.gov. An account is required to log in. The steps after logging in are:

* Select TOVS product, AMSU-A, Level 1B.

* Select date range desired

* Download using ncftp into /rgroup/amsu/noaa_18/ (similar for N19).

* Use "mget -f". The -f option forces overwrite of files.

* Remove the "NSS.AMAX." added at beginning of file names.

The original N18 orbit files are in directory/rgroup/amsu/noaa_18/. Similary

for N19. The automated cron program /rstor/braswell/reformat_amsu/go.bash computes the .a files and puts them in the dot_a_file directory.

The next step is to make a new file "orbit_file_list" by running “mk_new_orbit_file_list.perl” in the directory /rgroup/amsu/.

We are now ready to perform the processing that creates the new monthly grid files. In ~/ver6/amsu_v6/, update the dates to be processed in “run_amsu.sh” and run it. Note it can also be run from command line (eg):

a.out N18 2016 5 2016 5

a.out N19 2016 5 2016 5

After creation of the new grids, visually inspect them using the python program “image.py”. The month and satellite and channel to be displayed are set by editing image.py .

5.2.2 Update Two-Line-Element Database and Satellite Incidence Angles

To update the "flyer" record, add the latest TLE's to the satellite files (e.g. n18.txt, n18.txt) in directory ~/ver6/merge_v6/data_files/. The TLE's are obtained from www.space-track.org (an account is required to log on). This applies to : N18(NN 28654) and N19(NP 33591). Use cut and past to copy the TLE's. How we do it is to start to copy a region, then press and hold "shift" , then click at end of the region. This will select all of the TLE's. The new TLE's are appended to the end of the satellite files (n18.txt, n19.txt).

The next step is to update the file “valid_sat_months.txt” to show the latest month as now being valid. This file is in directory ~/ver6/merge_v6/.

Next, update the years to be processed in the program “main.flyer.f90”. This only has to be done if in a new year. The final steps are to compile and run the program:

* Compile with go.flyer.sh (creates a.out).

* Run(a.out) which creates the file “incidence_angles.dat”

5.2.3 Satellite Merge Processing and Output Products

The final processing is performed in directory ~/ver6/merge_v6/. In program "main.f90", update the parameters "end_year" and "end_new_year", if needed. Also make sure the data products directories exist that correspond to the name set in the program. To compile and run the program:

* Compile main.f90 with go.sh (creates a.out)

* Run main.f90 (a.out) to create the new products.

Next, visually check the created data products using the python programs

"image.py", "image1.py" or "image.5year.py ." Then use "uahncdc.py" to view a timeseries for the data. These programs are all included with the software.

The last step is to verify a new month really did get added to the uahncdc* files.

5.3 Quality Assessment and Diagnostics

The quality of the output products is continually assessed in two basic ways. First, the standard error of the differences of the co-orbiting satellites is followed with each month's run to check that the values are consistent and small. If a change occurs (i.e. an increasing standard error) this is usually a sign that a satellite's sensor is experiencing problems and will be investigated. In a number of cases (e.g. NOAA-14, NOAA-15, AQUA) this led to the cessation of utilizing data from the offending satellite from that point forward. Secondly, there will be routine comparisons between the UAH products and satellite-equivalent products from independent sources (i.e. radiosonde and Reanalyses datasets). Generally speaking, when a consistent difference between the UAH product and several of the independent products is discovered, an investigation will commence to determine the source of the differences.

5.4 Exception Handling

Not applicable in general. Some satellite data series are truncated due to excessive noise, but these are hard-wired into the code as termination of those particular time series.

5.5 Algorithm Validation

Extensive testing was done at every stage of code development to assure the intermediate results were correct and unchanged as the code was built into the final version. The direct validation is the most useful by comparing the output products from the UAH execution with the output products from execution at new site. If differences occur, the intermediate output files would be compared until the section of processing is discovered which creates differences between UAH and the new site. The data may first be

a comparison of images (i.e. global maps of anomalies) followed by a comparison of the numerical output.

5.6 Processing Environment and Resources

Operating System: Redhat Enterprise 7.3, 64-bit

Programming languages: Fortran 90

Compiler: Portland Group Fortran 90, ver 16.3-0, 64 bit

External libraries: Lapack (ver lapack-3.4.2-5.el7.x86_64)

Blas (ver blas-3.4.2-5.el7.x86_64)

Resource Usage:

AMSU grid generation:

CPU time – 39 sec

Wall time – 56 sec

Temporary storage(max) 92,804K

Merge Processing:

CPU time – 486 sec

Wall time – 554 sec

Temporary storage(max) – 3,848,764K

6. Assumptions and Limitations

6.1 Algorithm Performance

There are many problems which can arise in spaceborne measurements from passive microwave radiometers like AMSU, too many to be anticipated. The processing described here assumes the instruments are operating nominally.

If there is a channel failure, we decide how it should be handled based upon what other data are available, and how necessary the channel is to our processing. So far, we have not had a catastrophic failure of any of the primary channels used for our products, which are AMSU channels 5, 7, and 9. There have been periods of up to several days were satellite data were lost somewhere in the communications system, but unrelated to our activities. As of this writing, and with the exception of some gaps just mentioned, we have always had at least one radiometer operating since 16 Nov 1978. Some sensors have experience sufficient problems that we halted their use early (TIROS-N, NOAA-9 channel 2, NOAA-16) but a co-orbiting satellite has always been available to keep the time series continuous and connectable to the previous satellites.

At this writing, we had abandoned the Aqua AMSU channel 5 in 2009 due to increasing noise.

6.2 Sensor Performance

There are many problems which can arise in spaceborne measurements from passive microwave radiometers like AMSU, too many to be anticipated. The processing described here assumes the instruments are operating nominally.

If there is a channel failure, we decide how it should be handled based upon what other data are available, and how necessary the channel is to our processing. So far, we have not had a catastrophic failure of any of the primary channels used for our products, which are AMSU channels 5, 7, and 9. There have been periods of up to several days were satellite data were lost somewhere in the communications system, but unrelated to our activities. As of this writing, and with the exception of some gaps just mentioned, we have always had at least one radiometer operating since 16 Nov 1978. Some sensors have experience sufficient problems that we halted their use early (TIROS-N, NOAA-9 channel 2, NOAA-16) but a co-orbiting satellite has always been available to keep the time series continuous and connectable to the previous satellites.

At this writing, we had abandoned the Aqua AMSU channel 5 in 2009 due to increasing noise.

7. Future Enhancements

We continue to examine possible evidence for small residual drifts in one or more satellites. It is not known at this point what enhancements will be performed with a future dataset version.

8. References

Christy, J.R., R.W. Spencer and W.B Norris (deceased), 2011: The role of remote sensing in monitoring global bulk tropospheric temperatures. Int. J. Remote Sens. 32, 671-685, DOI:10.1080/01431161.2010.517803.

Christy, J.R., B. Herman, R. Pielke, Sr., P. Klotzbach, R.T. McNider, J.J. Hnilo, R.W. Spencer, T. Chase and D. Douglass, 2010: What do observational datasets say about modeled tropospheric temperature trends since 1979? Remote Sens. 2, 2138-2169. Doi:10.3390/rs2092148.

Christy, J.R. and W.B. Norris, 2009: Discontinuity issues with radiosondes and satellite temperatures in the Australian region 1979-2006. J. Atmos. Oc. Tech., 26, 508-522, DOI: 10.1175/2008JTECHA1126.1

Christy, J.R., W.B. Norris, R.W. Spencer, and J.J. Hnilo (2007). Tropospheric temperature change since 1979 from tropical radiosonde and satellite measurements. J. Geophys. Res., 112, D06102, 16 pp.

Christy, J.R. and W.B. Norris, 2006: Satellite and VIZ-Radiosonde intercomparisons for diagnosis on non-climatic influences. J. Atmos. Oc. Tech., 23, 1181 – 1194.

Christy, J.R., R.W. Spencer, W.B. Norris, W.D. Braswell and D.E. Parker (2003). Error Estimates of Version 5.0 of MSU–AMSU Bulk Atmospheric Temperatures. Journal of Atmospheric and Oceanic Technology: 20, pp. 613–629.

Christy, J.R., R.W. Spencer, W.B. Norris, W.D. Braswell and D.E. Parker (2002). Error Estimates of Version 5.0 of MSU/AMSU Bulk Atmospheric Temperatures. J. Atmos. Ocean. Tech., 20, 613-629.

Christy, J.R., R.W. Spencer, and W. D. Braswell (2000). MSU tropospheric temperatures: Dataset construction and radiosonde comparisons. J. Atmos. Ocean. Tech., 17, 1153-1170..

Christy, J.R., R.W. Spencer, and E.S. Lobl (1998). Analysis of the merging procedure for the MSU daily temperature time series. J. Climate, 11, 2016-2041.

Spencer, R.W., J.R. Christy and W.D. Braswell (2017). UAH Version 6 global satellite temperature products: Methodology and results (2017). Asia-Pac J. Atmos. Sci, 53(1), 121-130. DOI:10.1007/s13143-017-0010-y,

Spencer, R.W., J.R. Christy, W.D. Braswell, and W.B. Norris (2006). Estimation of tropospheric temperature trends from MSU channels 2 and 4. J. Atmos. Ocean. Tech, 23, 417-423

Spencer, R.W., J.R. Christy, and N.C. Grody (1996). Analysis of "Examination of 'Global atmospheric temperature monitoring with satellite microwave measurements'". Climatic Change, 33, 477-489.

Spencer, R.W. (1994). Global temperature monitoring from space. Adv. Space Res., 14, (1)69-(1)75.

Spencer, R.W. (1993). Monitoring of global tropospheric and stratospheric temperature trends. Atlas of Satellite Observations Related to Global Change, Cambridge University Press.

Spencer, R.W., and J.R. Christy (1993). Precision lower stratospheric temperature monitoring with the MSU: Technique, validation, and results 1979-91. J. Climate, 6, 1301-1326.

Spencer, R.W., and J.R. Christy (1992a). Precision and radiosonde validation of satellite gridpoint temperature anomalies, Part I: MSU channel 2. J. Climate, 5, 847-857.

Spencer, R.W., and J.R. Christy (1992b). Precision and radiosonde validation of satellite gridpoint temperature anomalies, Part II: A tropospheric retrieval and trends during 1979-90. J. Climate, 5, 858-866.

Spencer, R.W., J.R. Christy, and N.C. Grody (1990). Global atmospheric temperature monitoring with satellite microwave measurements: Method and results, 1979-84. J. Climate, 3, 1111-1128.

Spencer, R.W., and J.R. Christy (1990). Precise monitoring of global temperature trends from satellites. Science, 247, 1558-1562.

Appendix A. Acronyms and Abbreviations

Acronym or Abbreviation	Definition
AMSU	Advanced Microwave Sounding Unit
ANSI	American National Standards Institute
C-ATBD	Climate Algorithm Theoretical Basis Document
CDR	Climate Data Record
IEEE	Institute of Electrical and Electronic Engineers
ICD	Interface Control Document
IOC	Initial Operating Capability
FOC	Full Operating Capability
MetOp	European Space Agency Polar Orbiting Meteorological Satellite
MLT	Mean Layer Temperature
MSU	Microwave Sounding Unit
NCDC	National Climatic Data Center
NCEI	National Centers for Environmental Information
NOAA	National Oceanic and Atmospheric Administration
OAD	Operational Algorithm Description
PRT	Platinum Resistance Thermometer
Tb	Brightness Temperature
TLS	Temperature of the Lower Stratosphere
TLT	Temperature of the Lower Troposphere
TMT	Temperature of the Mid-Troposphere
TTP	Temperature near the TropoPause
UAH	University of Alabama in Huntsville